C Journal of Carbon Research

MDPI

Article

Sustainable Supercapacitors Based on Polypyrrole-Doped Activated Biochar from Wood Waste Electrodes

Ravi Moreno Araujo Pinheiro Lima [1,†], Glaydson Simões dos Reis [2,*,†], Ulla Lassi [3,4,*], Eder Claudio Lima [5], Guilherme Luiz Dotto [6] and Helinando Pequeno de Oliveira [1,*]

1 Institute of Materials Science, Federal University of Sao Francisco Valley, Juazeiro 48902-300, Bahia, Brazil; raviplima.engmec@gmail.com
2 Department of Forest Biomaterials and Technology, Swedish University of Agricultural Sciences, Biomass Technology Centre, SE-90183 Umeå, Sweden
3 Research Unit of Sustainable Chemistry, University of Oulu, FI-90014 Oulu, Finland
4 Unit of Applied Chemistry, University of Jyvaskyla, Kokkola University Consortium Chydenius, Talonpojankatu 2B, FI-67100 Kokkola, Finland
5 Institute of Chemistry, Federal University of Rio Grande do Sul–UFRGS, Av. Bento Gonçalves 9500, P.O. Box 15003, Porto Alegre 91501-970, RS, Brazil; profederlima@gmail.com
6 Research Group on Adsorptive and Catalytic Process Engineering (ENGEPAC), Federal University of Santa Maria, Av. Roraima, 1000-7, Santa Maria 97105–900, RS, Brazil; guilherme_dotto@yahoo.com.br
* Correspondence: glaydson.simoes.dos.reis@slu.se (G.S.d.R); ulla.lassi@oulu.fi (U.L.); helinando.oliveira@univasf.edu.br (H.P.d.O.)
† These authors contributed equally to this work.

Abstract: The synthesis of high-performance carbon-based materials from biomass residues for electrodes has been considered a challenge to achieve in supercapacitor-based production. In this work, activated biochar has been prepared as the active electrode material for supercapacitors (SCs), and an effective method has been explored to boost its capacitive performance by employing polypyrrole (PPy) as a biochar dopant. The results for physicochemical characterization data have demonstrated that PPy doping affects the biochar morphology, specific surface area, pore structure, and incorporation of surface functionalities on modified biochar. Biochar-PPy exhibited a surface area of 87 m^2 g^{-1}, while pristine biochar exhibited 1052 m^2 g^{-1}. The SCs were assembled employing two electrodes sandwiched with PVA solid-state film electrolyte as a separator. The device was characterized by standard electrochemical assays that indicated an improvement of 34% in areal capacitance. The wood electrodes delivered high areal capacitances of 282 and 370 mF cm^{-2} at 5 mA cm^{-2}, for pure biochar and biochar doped with PPy, respectively, with typical retention in the capacitive response of 72% at the end of 1000 cycles of operation of the supercapacitor at high current density, indicating that biochar-PPy-based electrode devices exhibited a higher energy density when compared to pure biochar devices.

Keywords: wood waste; wood electrodes; wood-based supercapacitors; polypyrrole; pseudocapacitance

Citation: Lima, R.M.A.P.; dos Reis, G.S.; Lassi, U.; Lima, E.C.; Dotto, G.L.; de Oliveira, H.P. Sustainable Supercapacitors Based on Polypyrrole-Doped Activated Biochar from Wood Waste Electrodes. *C* **2023**, *9*, 59. https://doi.org/10.3390/c9020059

Academic Editors: Nikolaos Kostoglou and Claus Rebholz

Received: 3 May 2023
Revised: 28 May 2023
Accepted: 1 June 2023
Published: 5 June 2023

1. Introduction

The growing global population, the depletion of natural resources, and the negative impact of industrial manufacturing processes are driving factors for the increasing demand for more sustainable manufacturing processes and products for the energy storage industry. As a consequence, scientists have explored solutions for sustainable materials and products for greener storage devices through a tenfold increase in scientific publications in 2010–2020 [1–5].

Due to the diversity of the required small and large energy systems, the development of electrochemical energy storage devices, such as supercapacitors (SCs) and batteries, has been extensively reported in the literature; batteries have higher energy densities at the cost of low power densities, while SCs are characterized by high power densities and

low energy densities, with the advantages of having a high power capacity and being endowed with fast charging/discharging cycles [6], light weight [5], and both economic and environmental advantages such as the use of aqueous electrolytes [2]. SCs have a huge relevance for applications such as electrical automobiles [7] and telecommunications [8] by integrating strategies based on the incorporation of solar electricity or the harvesting of mechanical movement converted into electricity [5,9,10].

The optimal configuration of supercapacitors has been explored with the combination of porous electrodes and electrolytes to improve the charge separation at the Helmholtz double layer and the electrode–electrolyte interface [4]. Supercapacitors are composed of electrodes that depend on features such as high specific surface area, surface chemistry, and electrical conductivity [11]. To date, several materials (e.g., graphite [12], metal oxides/hydroxides [13], and conducting polymers [14]) have been employed as high-performance electrodes for SCs. On the other hand, two-dimensional nanostructures (graphene, MXene, metal dichalcogenides) present outstanding properties such as high package density, high surface area, transparency, and chemical/mechanical stability that enable their use in supercapacitors [15]. Despite these advantages, the typical stacking/aggregation of 2D structures reduces the electrochemical performance of the devices. To circumvent these drawbacks, different strategies have focused on the exfoliation of black phosphorous [16] and on the surface modification of structures with nitrogen, sulfur, and phosphorous-based groups (heteroatom doping strategies) that reinforce the pseudocapacitance of the resulting material [17]. The incorporation of materials with characteristic redox reactions is another important strategy that is conducted given the fast electrochemical kinetics in systems such as vanadium redox flow batteries [18] and with the incorporation of carbonaceous materials to avoid corrosive and degradative processes in Zn anodes [19].

However, these electrode materials have the drawbacks of high production costs and/or non-eco-friendly fabrication methods. Thus, it is crucial to develop electrode materials with the properties of sustainability, eco-friendly behavior, low cost, and efficient response. In this direction, carbon electrodes from biomass precursors have attracted huge attention due to their worldwide availability and abundance, non-toxicity, and high surface area with hierarchical porous structure materials [20,21] to improve the mechanisms of efficient charge separation.

Pyrolysis is a standard method to convert biomass into porous materials whose properties are highly dependent on the pyrolysis conditions and the chemicals used for the activation or doping processes [22–24]. For instance, nitrogen doping methods in carbon preparation for SCs have been shown to boost its conductivities and hydrophilicity, which improve its surface wettability, resulting in an increased pseudocapacitance effect, thus delivering improved energy/power densities.

One of the ways to improve the electrochemical conductivity of carbon-based electrodes is coating with conducting polymers [25–27], such as polypyrrole (PPy), which is one of the most promising support materials due to its excellent electrical conductivity, environmental and thermal stability, and easy procedure of preparation [28–32]. Thus, it enables a promising possibility for the development of low-cost and commercially viable SCs.

The general mechanisms that are combined in the improvement of the electrochemical efficiency of the electrodes are based on two important processes: the electrical double layer capacitance (EDLC) acquired from the adsorption of electrolyte ions on conductive electrodes [33] and pseudocapacitive effects that allow good performance in energy storage through reversible redox on electrodes [34]. The adequate combination of EDLC and the pseudocapacitive effect in SCs improves the overall energy density of the devices by the combination of available sites for charge accumulation of EDLC and the rapid ionic transport of pseudocapacitive prototypes provided by the PPy-based biochar doping [35–37].

Herein, we aimed to explore the use of birch wood to produce porous biochar to be used as carbon electrodes for high-performance supercapacitors. Moreover, the prepared porous biochar was subjected to a polypyrrole, and its effect on both physicochemical and electrochemical properties was fully investigated. The obtained results suggest an

improved efficiency of the polypyrrole-doped biochar due to the pseudo-capacitive effect and the feasibility of the proposed approach for the fabrication of sustainable SCs based on biomass wastes.

2. Materials and Methods

2.1. Materials

Polyvinylidene fluoride (PVDF), cetyl trimethyl ammonium bromide (CTAB), dimethylformamide (DMF), and pyrrole (PPy) were obtained from Sigma Aldrich (St. Louis, MO, USA). Ammonium persulfate (APS) was obtained from Química Moderna (Barueri, SP, Brazil). Carbon black was purchased from Micromeritics (Norcross, GA, USA). All materials were used as received, except for the pyrrole, which was distilled before use.

2.2. Biochar Preparation

The biochar was prepared using birch wood wastes as a precursor. First, 20.0 g of the dried biomass was mixed with H_3PO_4 (50%) at a ratio of 1:4 (weight) and mixed until forming a homogeneous paste [38,39]. Then, the paste was kept at room temperature for 2 h and dried at 105 °C overnight. The dried paste was pyrolyzed at 700 °C for 2 h under an N_2 atmosphere, with an initial heating rate of 10 °C per min. The pyrolyzed material was ground and washed several times with boiling water until the pH value of the filtrate water was similar to the ultra-pure water.

2.3. Preparation of Birch-PPy Powder

The birch-PPy powder was prepared according to the procedure described as follows: birch powder was dispersed into 5 mL of Milli-Q water by sonication. Meanwhile, another solution containing polypyrrole and CTAB was prepared as follows: 35 uL of pyrrole was added into 5 mL of Milli-Q water and also incorporated with 9.6 mg of CTAB. This solution was stirred until the complete dispersion of the CTAB and mixed into the solution containing birch biochar to prepare solution A. After this, solution B was prepared by adding 114.6 mg of APS into 5 mL of milli-Q water. Then, solution A was stirred in an ice bath and received solution B (dropwise) in a process that initiated the polymerization. After 2 h of reaction, the dark solution was centrifuged at 5000× *g* for 5 min to obtain the precipitated particles. The black powder was filtered and washed several times with Milli-Q water to remove any residue from the polymerization process and was dried in an oven at 40 °C for 1 h. Finally, the birch-PPy at ambient temperature was stored for use. The loaded mass of polypyrrole in the composite was 11 mg.

2.4. Fabrication of the Biochar SCs Electrodes

Graphite paper (1 × 1 cm) was used as a support for the coating with the biochar-based material slurries, prepared with a mass ratio of 8:1:1 (biochar:PVDF:carbon black) as follows: 10 mg of PVDF was added to 500 µL of DMF and then heated to 60 °C and stirred until the PVDF was completely dispersed. After this step, 80 mg of birch biochar and 10 mg of carbon black were added to the mixture, which was kept under continuous stirring at 60 °C to provide a homogeneous dispersion of the carbonaceous derivative. The preparation of the electrode, after this step, was conducted as follows: First, 20 µL of the as-prepared slurry was dropped and spread on the substrate. Then, the coated graphite paper was heated at 50 °C to eliminate the residues of the solvent. The biochar-PPy-based electrodes were prepared using the same method, although instead of using the pure birch biochar, the composite biochar-PPy was used for the preparation of the slurry.

2.5. Electrolyte Preparation and Supercapacitor Assembly

Polyvinyl alcohol (PVA) was explored as a solid-state film for the preparation of the electrolyte. The standard procedure for preparation was conducted as follows: First, 1 g of PVA was added into 10 mL of Milli-Q water and heated to 70 °C under stirring for 1 h. After this, the temperature was raised to 100 °C, and the solution was stirred for an

additional 1 h. Then, a transparent aspect of the solution was observed, and the solution was cooled to room temperature. As a following step, the solution was stirred for 15 min and received 1 mL of H_3PO_4. To avoid bubbles, the solution was sonicated for 2 min. Then, the solution was placed in a mold, and a thin film of PVA was obtained after 48 h. The PVA film was cut into pieces with 1 cm^2 of area and used as a solid-state electrolyte. The SCs were assembled in a sandwich configuration in which two electrodes were placed parallel to each other, separated by the PVA solid electrolyte film.

2.6. Characterization

The morphology evaluation of the biochars was carried out using a scanning electron microscope Vega 3XM (Tescan) with an electron acceleration of 10 kV, with the collected images collected with magnifications of 500 x, 1 kx, 3 kx, and 5 kx. The chemical composition of the materials was evaluated from Fourier transform infrared spectrum (FTIR) using the KBr method in an IR Prestige-21 Fourier transform infrared spectrometer (Shimadzu).

The specific surface area and pore volume of the biochar materials were measured through N_2 adsorption-desorption via the BET (Brunauer, Emmett and Teller) and BJH (Barrett-JoynerHalenda) method, respectively, on a Surface Area Analyzer (ASAP 2020, Micromeritics).

Electrochemical characterization of the supercapacitors explored the two-electrode configuration with measurements provided by a potentiostat Autolab PGSTAT 302 N (Methrom) for the acquisition of voltammetry curves at different scan rates (10 mV s^{-1} to 200 mV s^{-1}), with a potential window range of 0 to 0.8 V. Galvanometric curves was performed with a current density ranging from 1 mA to 5 mA, and the impedance spectrum was evaluated in a frequency range of 1 Hz to 1 MHz with data fitted by modified Randles circuit using the software Zview 2 version 3.4.

The areal capacitance was calculated from galvanostatic curves, as follows:

$$C_a = \frac{2A_{discharge} \times I}{V^2 \times A_{electrode}} \quad (1)$$

where $A_{discharge}$ is the area of the discharge curve, I is the current applied, V is the potential relative to the beginning of the discharge curve (below the IR drop), and $A_{electrode}$ is the area of the electrode.

To obtain the Ragone data, the calculus of the energy and power density was provided by Equations (2) and (3):

$$E_d = \frac{C_a \times V^2}{2 \times 3600} \quad (2)$$

$$P_d = \frac{3600 \times E_d}{\Delta t} \quad (3)$$

where E_d is the energy density (W h cm^{-2}), P_d is the power density (W cm^{-2}), C_a is the areal capacitance obtained from Equation (1), and Δt is the discharge time.

3. Results and Discussion

3.1. Characterization of the Biochar and Biochar-PPy Electrode Materials

The surface morphology of the biochar and biochar doped with PPy was evaluated from SEM analyses. The SEM images at different magnifications are shown in Figure 1. The pristine biochar (Figure 1a) is characterized by a dense distribution of particles with a low concentration of small grains on its surface, while biochar doped with polypyrrole (see Figure 1b) shows an evident change in morphology due to the coating of biochar by aggregates of grains of polypyrrole (a typical disposition of PPy grains), showing that the doping process provoked important changes in the biochar morphology. Such difference is evidence of the adherence of polypyrrole on biochar's surface, which could create both defects in biochar structure and nitrogen functionalities (from PPy) that can boost its electrochemical performances [40]. Overlaid EDS images in Figure 1c,d for biochar and

biochar-PPy, respectively, confirm the higher density of nitrogen-based groups by coating with polypyrrole (green dots are attributed to carbon and red dots to nitrogen), confirming the adequate modification with PPy.

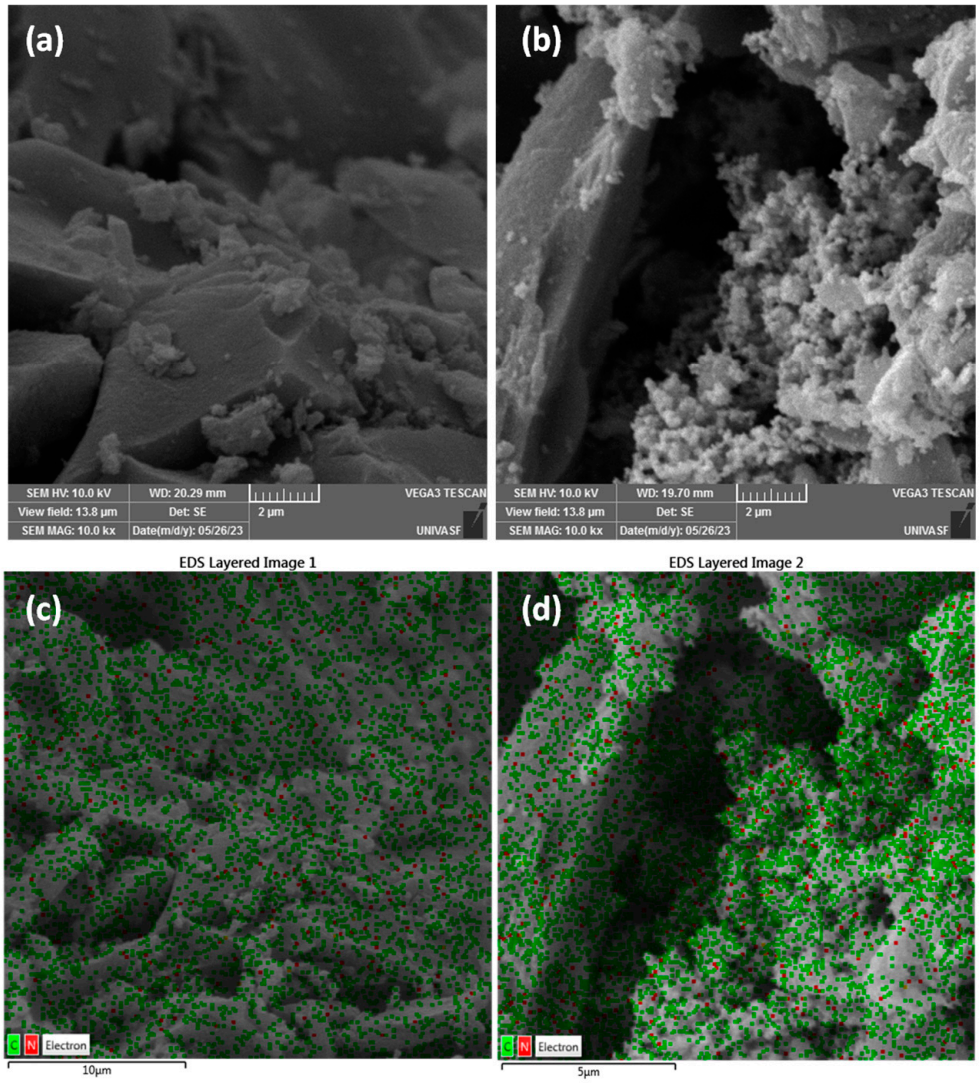

Figure 1. SEM images for birch biochar (**a**) and biochar doped with PPy (**b**), and overlaid EDS images (red dots for nitrogen element and green dots for carbon element) for biochar (**c**) and biochar doped with PPy (**d**).

Images for as-prepared electrodes of biochar (Figure 2a) and biochar doped with PPy (Figure 2b) correspond to the images reported for composites (Figure 1) in which a dense distribution of grains is observed for the coated material (incorporation of PPyon biochar). After 1000 cycles of use, the electrodes were re-evaluated (images shown in Figure 2c (biochar) and Figure 2d (biochar +PPy)), indicating a more compact structure with a reduction in the size of grains of biochar and compressed grains of polypyrrole, as a result of the compressive forces during measurement and the smoothness of polypyrrole. No cracks of microstructural changes were observed as a result of the electrochemical characterization.

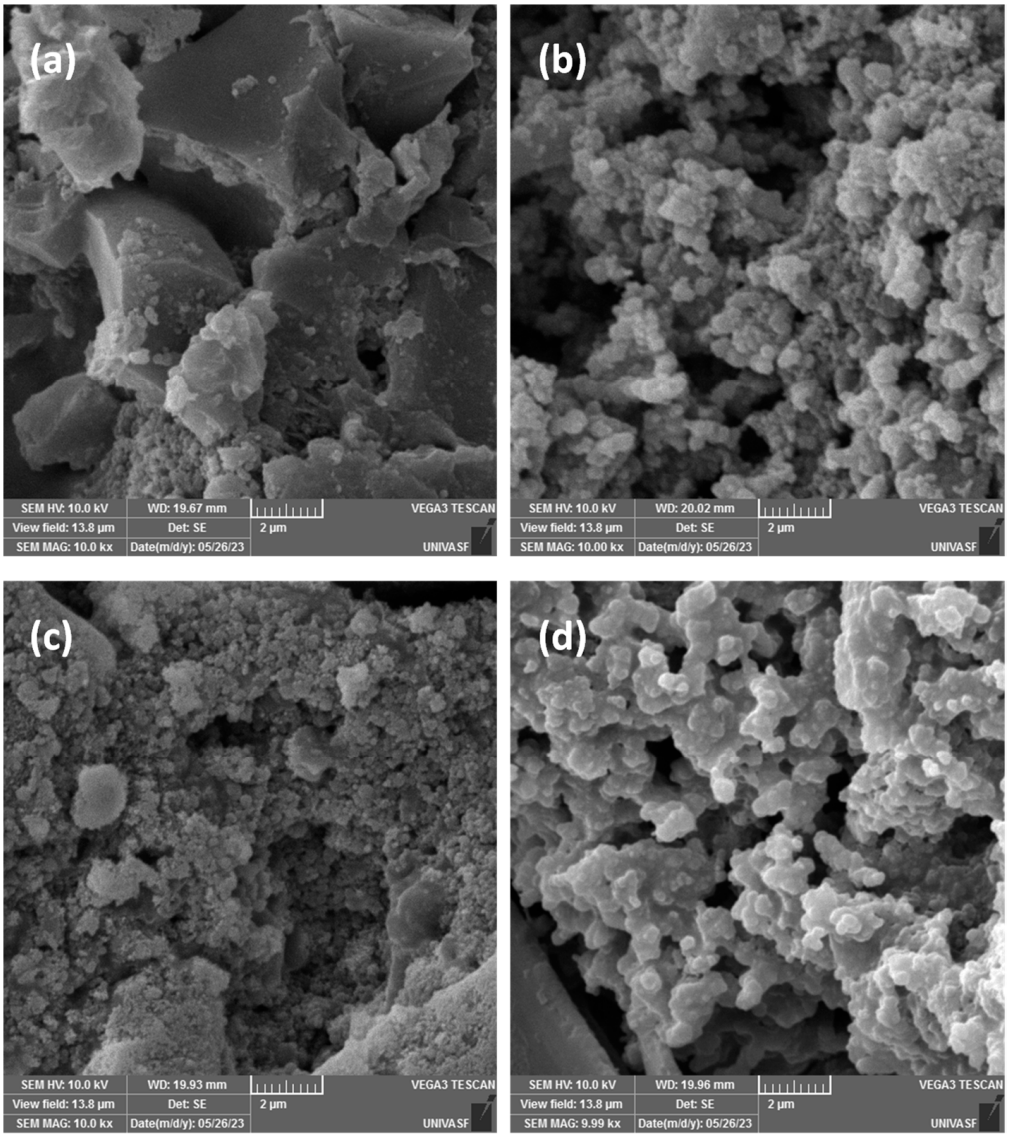

Figure 2. Comparison between SEM images for electrodes before use of birch biochar (**a**) and biochar doped with PPy (**b**), and after 1000 cycles of operation—birch biochar (**c**) and biochar doped with PPy (**d**).

The pore structure and the change in the porosity degree before and after PPy doping were evaluated following the N_2 adsorption/desorption as shown in Figure 3. The N_2 adsorption-desorption isotherms of biochar (Figure 3a) and biochar-PPy (Figure 3b) show that the PPy doping provoked a high impact on their shapes and the amount of adsorbed N_2. According to the IUPAC classification [41], the non-doped biochar shows an isotherm that seems to be a mix of types I and IV; type I is related to the presence of micropores due to the high N_2 adsorption at low partial pressure, and type IV since it shows hysteresis from partial relative pressure of 0.4, which is a strong indication of the presence of mesoporosity [23,42]. The biochar doped with PPy shows a clear isotherm type IV [41]. Moreover, the deposition of PPy on biochar structure seems to reduce the porosity of the biochar-PPy due to reduced adsorbed N_2 volume: 458.0 $cm^3\ g^{-1}$ and 57.0 $cm^3\ g^{-1}$ for biochar and biochar-PPy, respectively.

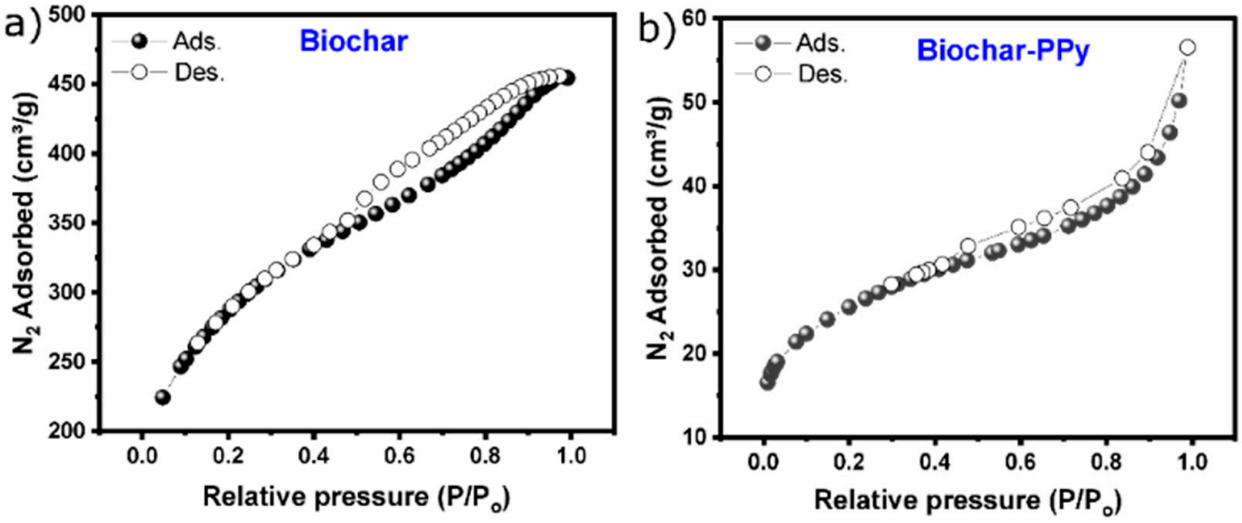

Figure 3. Nitrogen (N_2) adsorption/desorption isotherms of (**a**) biochar and (**b**) Biochar-PPy.

The SSA and porosity values of the biochar electrodes are shown in Table 1. Biochar-PPy had a surface area of 87 m^2 g^{-1}, which is much lower than that of pristine biochar (1052 m^2 g^{-1}) (see Table 1). The decrease in the SSA and pore volume was due to the deposition of PPy on the carbon structure that covered the highly porous surface of the biochar sample.

Table 1. Textural properties of the biochar samples.

Samples	SSA (m^2 g^{-1})	A_{Micro} (m^2 g^{-1})	A_{Meso} (m^2 g^{-1})	Pore Volume (cm^3 g^{-1})
Biochar	1052	240	812	0.46
Biochar-PPy	87	21	66	0.072

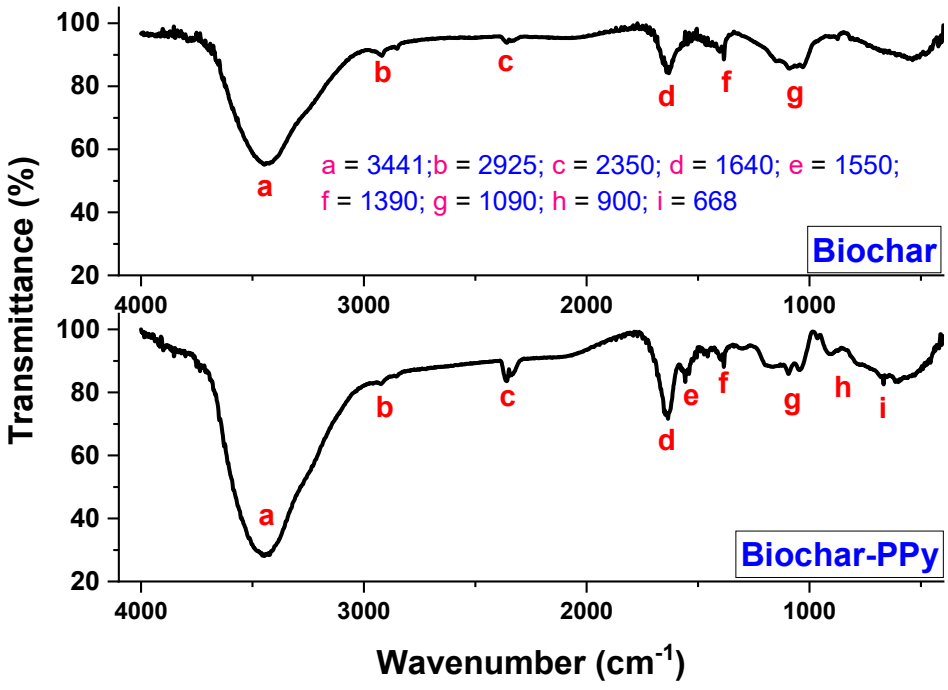

Figure 4. FTIR spectra of biochar and biochar-PPy samples.

The reduction of SSA can be beneficial for SC performance since the pseudocapacitance of polypyrrole prevails on the EDLC performance of carbon derivatives, which is surface area dependent. As expected, the insertion of PPy and N-functionalities can boost the pseudocapacitance of the biochar-PPy through redox reactions.

FTIR spectra were evaluated to examine the presence of surface functionalities on biochar surfaces, as well as the impact of PPy doping on the resulting material. FTIR spectra of biochar and biochar modified with PPy are shown in Figure 4. It is observed that the PPy doping caused an impact on biochar's surface functionalities. The absorption bands at 3441 cm^{-1} may be attributed to the O−H stretching vibration and are broader in biochar-PPy. The small peak at 2925 cm^{-1} is related to symmetric vibrations of the CH_2 units [43]. The peak at 1640 cm^{-1} is due to the stretching vibrations of the C=O and C=C units [44]. The spectrum of the biochar-PPy exhibited characteristic peaks at 1550, 900, and 668 cm^{-1}, which are indexed to the C=C stretching, C–N stretching, and C–N in-plane deformation, respectively, indicating the presence of a doped PPy state [45]. The above outcomes suggest that the biochar-PPy material was successfully prepared.

3.2. Electrochemical Assays

The electrochemical performance of supercapacitors can be successfully evaluated by cyclic voltammogram (CV) and galvanostatic charge/discharge (GCD) analyses. CV profiles of the biochar and biochar doped with PPy were evaluated using the electrochemical cell in which supercapacitor prototypes are sandwiched in parallel, plated, and characterized at scan rates ranging from 10 to 200 mV s^{-1} (see Figure 5a,b). Both curves show that square-shaped aspects are more pronounced at a lower scan rate. At increasing scan rates, the oblate aspect of the curves can be assigned to the pseudocapacitive behavior of additives. In terms of the maximum value of the current at a corresponding value of the scan rate, it is possible to observe that values for polypyrrole-based supercapacitors are higher than those observed for non-modified devices (biochar-based supercapacitors). As a consequence, the enclosed area in curves (applied as a parameter for the calculus of the areal capacitance) indicates that the incorporation of polypyrrole introduces changes in the electrochemical performance of the modified electrodes. These cone-shaped curves, observed at a high scan rate (200 mVs^{-1}), are attributed to the abundance of functional groups that are known to be present on biochars, especially biochars doped with PPy [44]. As expected, the incorporation of PPy in the structure contributes to reversible redox reactions that favor an increase in the overall capacitance and consequently in the energy density due to the facilitated transference of ions under the doping process in cycles of swelling/contraction of the conducting polymer chain.

The electrochemical performance of electrodes was further evaluated by using GCD curves (see Figure 5c,d). Both biochar and biochar-PPy showed slight deviations from the linear branch. For PPy-doped electrodes, a slight curvature is observed, indicating the reversible accumulation of charge and a pseudocapacitance effect due to the redox reaction provoked by the nitrogen functionalities on biochar-PPy. As expected, a complete charge-discharge takes longer characteristic times for supercapacitors under a lower current density regimen. The supercapacitor based on biochar-PPy displayed a total charge-discharge period in the order of 680 s, while pure biochar is in the order of 510 s (at a corresponding current of 1 mA), highlighting the importance of the polypyrrole doping on the overall SCs' performance. These results following CV analysis indicated a superior electrochemical performance for biochar doped with PPy.

The areal capacitances obtained from the GCD curves and calculated using Equation (1) (and shown in Figure 6a) confirm that for all of the current density ranges, the performance for PPy-modified biochar-based electrodes is better than that observed for pristine ones. The best performance in the overall range of current densities is the result of the combined good pseudocapacitive contribution and the high conductivity of the polymeric film. An interesting aspect to be considered from these results is that a slight reduction in the performance of biochar-based supercapacitors at increasing current density is circumvented

by a slight increase in the performance of PPy-modified biochars, which is clear evidence that operation at higher current density regimen is favored by the incorporation of a conducting polymer on devices. The corresponding variation for areal capacitance as a function of the scan rate is shown in Figure 6b. As can be seen, an overall reduction in the performance is observed in both experimental systems at increasing scan rate [37], with a general best performance for biochar-PPy samples, confirming the previous results from GCD data.

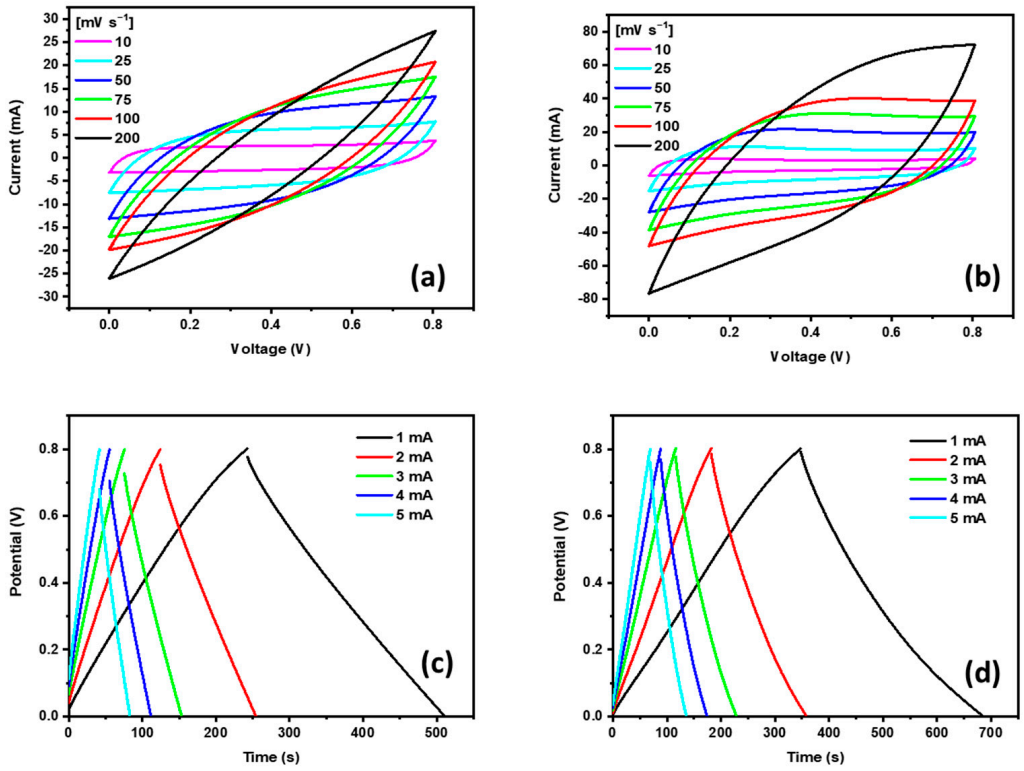

Figure 5. CV curves at different scan rates for biochar (**a**) and biochar-PPy-based electrodes (**b**), and GCD curves at various current densities for biochar (**c**) and biochar-PPy (**d**) electrodes.

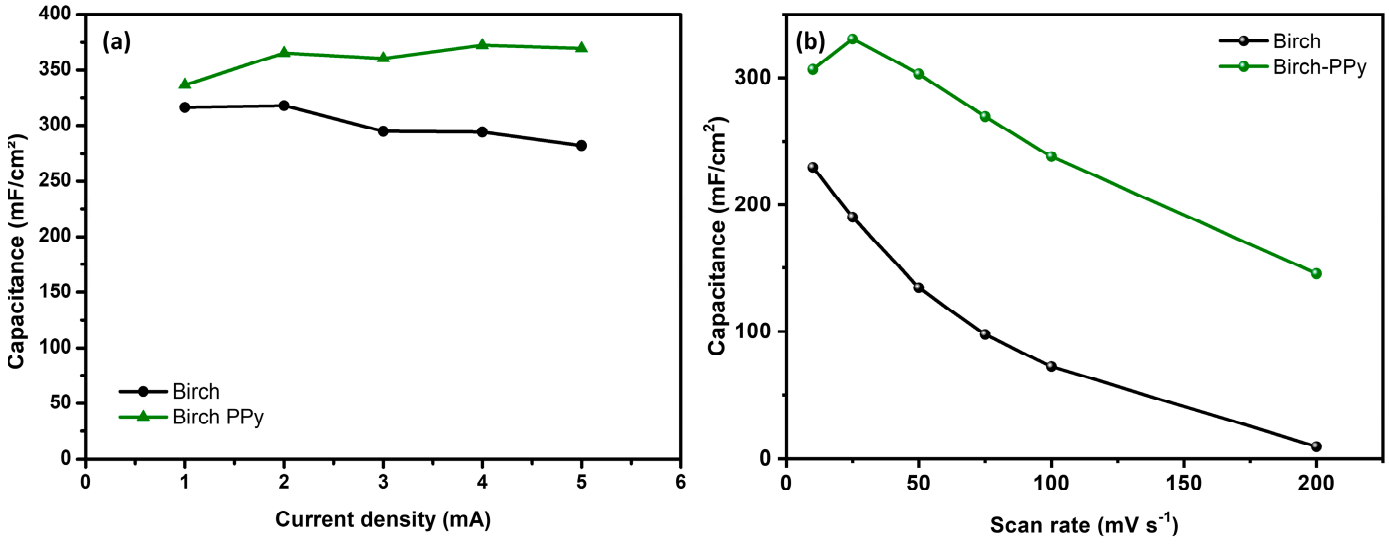

Figure 6. Areal capacitances at different current densities for supercapacitors based on biochar and biochar-PPy electrodes calculated from GCD curves (**a**) and corresponding variation of the areal capacitance as a function of the scan rate in CV curves (**b**).

The performance of modified supercapacitors introduces advantages in comparison with corresponding systems reported in the literature, such as polyaniline-doped graphene fiber [46] and $NiCo_2O_4$ thin film [47]. These materials presented complex synthesis routes and still presented poorer electrochemical properties in comparison with the experimental system reported in this work. A more complete comparison with different electrode materials is given in Table 2, which provides a comparison of the C_A values of several types of electrode materials. As can be seen, a good performance for non-doped and PPy-doped biochar electrodes is observed by direct comparison with supercapacitors prepared with different electrodes. These highlights indicate that birch wastes can be a low-cost, sustainable, and efficient precursor to fabricate high-performance electrodes for SCs application.

Table 2. The areal capacitance of different electrode materials in comparison with that of the present work.

Electrode Material	Areal Capacitance	Capacitance Retention/Cycle	Electrolyte	Current Density (A g^{-1}) or Scan Rate (mV s^{-1})	Ref.
Graphene fiber	3.3 mF cm^{-2}	-/5000	PVA/H_3PO_4	0.1 mA cm^{-2}	[46]
Polyaniline-doped graphene fiber	66.6 mF cm^{-2}	-/5000	PVA/H_3PO_4	0.1 mA cm^{-2}	[46]
$NiCo_2O_4$ thin film	40.6 mF cm^{-2}	96.5%/10,000	2 M KOH	0.133 mA cm^{-2}	[47]
MnO_2 /MoS_2	224 mF cm^{-2}	90%/3000	1.0 M Na_2SO_4	0.1 mA cm^{-2}	[48]
TiO_2	23.24 mF cm^{-2}	-/10,000	0.5 M Na_2SO_4	2 mV s^{-1}	[49]
Sheet-like $ZnCo_2O_4$	16.13	-/1000	1 M KOH	0.01 mA cm^{-2}	[50]
Carbon dots/graphene microfibers	607 mF cm^{-2}	-/2000	$EMIBF_4$/PVDF-HFP	20 mA cm^{-2}	[51]
MnO_2-modified hierarchical graphene fiber	9.6 mF cm^{-2}	-/1000	H_2SO_4–PVA	10 mV s^{-1}	[52]
Graphene modified with polyaniline	87.8 mF cm^{-2}	93%/10,000	EMITFSI/PVDF-HFP	0.22 mA cm^{-2}	[53]
MnO2@Au nanofiber	8.26 mF cm^{-2}	-/10,000	LiCl-PVA	5 mV s^{-1}	[54]
Carbon cloth-carbon fiber-TiO_2	270 mF cm^{-2}	-	1 M H_2SO_4	10 mA g^{-1}	[55]
2D-$LiCoO_2$	310 mF cm^{-2}	80.2%/2000	LiCl-PVA	5 mV s^{-1}	[56]
Carbon-doped titanium nitride	45.8 mF cm^{-2}	96%/5000	6 M KOH	10 mV s^{-1}	[57]
Nanoneedles-anchored CuCo-layered double hydroxide	7.02 mF cm^{-2}	96%/10,000	3 M KOH	30 mA cm^{-2}	[58]
Biochar	282 mF cm^{-2}	92%/1000	PVA solid-state film	5 mA cm^{-2}	This work
Biochar-PPy	370 mF cm^{-2}	72%/1000	PVA solid-state film	5 mA cm^{-2}	This work

The energy density and power density of the two SCs were obtained from Equations (2) and (3) and are shown in the Ragone plot (see Figure 7). As expected, the biochar-PPy-based electrode device showed the highest energy density. The PPy doping seemed to have increased its surface's polarity due to the presence of N-heteroatom functionalities, which boost electrostatic interactions between the electrode's active surface and the electrolyte ions, diminishing its equivalent resistance [59]. As expected, the improvement in the faradic

redox reactions contributes to pseudocapacitance and enhances the supercapacitor's energy density due to the polypyrrole incorporation. The comparison with reported values in the literature is shown in the Ragone plot.

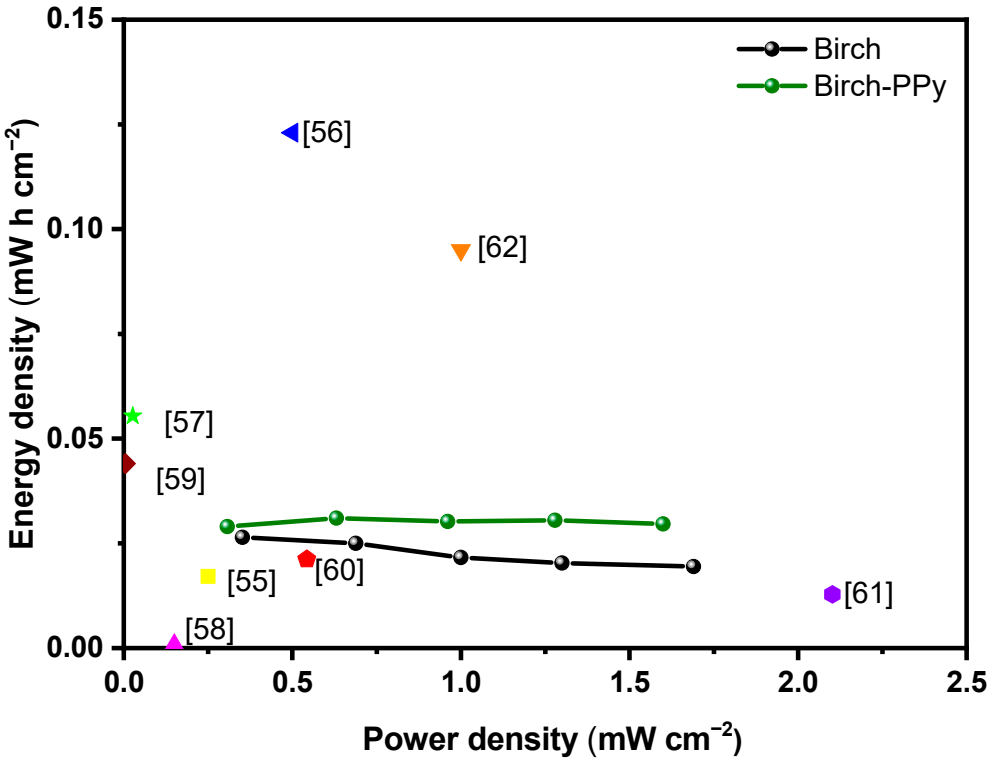

Figure 7. Ragone plot for biochar (curve in black) and biochar-PPy (curve in green) supercapacitors. For comparison, results from the literature are introduced in the colored dots: yellow [60], blue [61], green [62], magenta [63], wine [64], red [65], violet [66], and orange [67].

Another important characterization to be evaluated in supercapacitors is the measurement of the retention in the electrochemical properties of the materials under successive charge-discharge cycles. With this aim, successive charge-discharge cycles were imposed under two different currents (4 mA and 5 mA) in supercapacitors prepared with biochar (pristine) and doped by polypyrrole. After 1000 complete cycles of charge-discharge at a constant current density, Figure 8 summarizes the variation in the capacitance retention of the supercapacitors as a function of aging. In agreement with what was observed for carbonaceous materials, a slight linear decrease in the performance of the device is observed for a biochar-based supercapacitor with a value in the order of 93% retention in the electrochemical properties after 1000 cycles of use for both current densities. As expected, and as observed as a typical response for pseudocapacitive materials, reported for polypyrrole [68] and N-doping materials [17], a more pronounced decrease in the retention is observed for modified devices, which reach values in the order of 72% after 1000 cycles of use at 5 mA and 76.5% after 1000 cycles at 4 mA. Relative to the variation observed for these systems, it is worth observing that poor cycling performance is reported in the literature for polypyrrole-based supercapacitors [69], as a consequence of periodic contraction/expansion of polypyrrole chains under repeated anodic and cathodic polarization (under successive extraction/insertion of ions). These processes result in the formation of cracks that negatively affects the capacitance performance of the PPy-based devices. The incorporation of carbon-based materials minimizes the degradation rate since additives act as buffer space for polypyrrole volume variation.

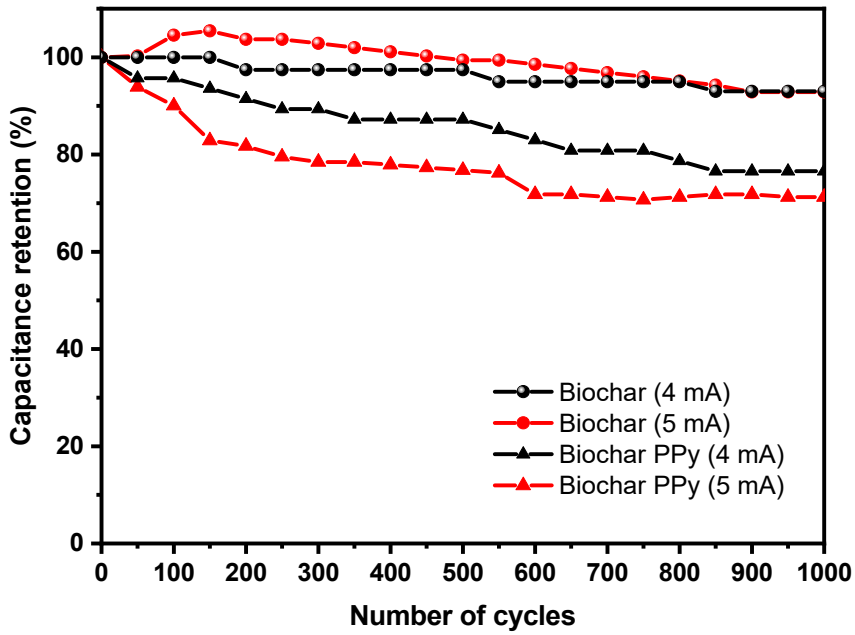

Figure 8. Comparison of retention in the capacitance after 1000 cycles of use of biochar at 4 mA (black dots), 5 mA (red dots), and biochar-PPy supercapacitors at 4 mA (black triangles) and 5 mA (red triangles).

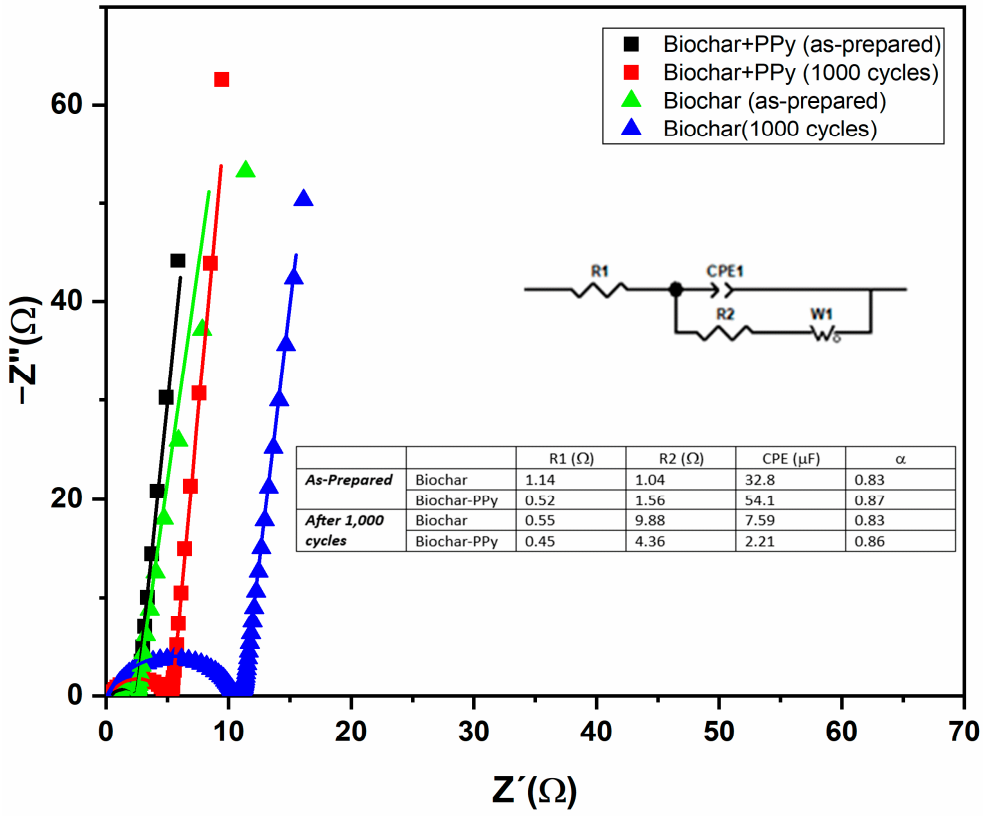

		R1 (Ω)	R2 (Ω)	CPE (μF)	α
As-Prepared	Biochar	1.14	1.04	32.8	0.83
	Biochar-PPy	0.52	1.56	54.1	0.87
After 1,000 cycles	Biochar	0.55	9.88	7.59	0.83
	Biochar-PPy	0.45	4.36	2.21	0.86

Figure 9. Nyquist diagram of both devices (0.01 Hz–1 MHz) for SCs composed with biochar and biochar-PPy samples characterized before and after the successive 1000 cycles of charge/discharge assays. The corresponding equivalent circuit (modified Randles circuit) and the corresponding fitting parameters for bulk resistance, charge transfer resistance, CPE, and parameter α are presented in the inset.

In addition, to further understand the intrinsic properties that influence the overall performance of the PPy-modified electrodes, electrical impedance spectroscopy (EIS) assays were conducted, in a frequency range from 0.01 Hz to 1 MHz, to further evaluate the behavior of biochar electrodes for supercapacitors (see Figure 9) before and after 1000 cycles of operation under conditions of high current (5 mA) and high degradation rate. The Nyquist plots of electrodes exhibit a semicircle and a straight line in the high and low-frequency regions, respectively, highlighting its capacitive behavior and ion diffusion [50]. The corresponding response for samples tested after 1000 cycles of charge/discharge shows a general shift to higher values of impedance in the diagram, confirming the degradation of the samples.

It is known that a longer diameter in the semicircle is attributed to a higher charge transfer resistance [40], and the biochar-PPy-based supercapacitor had a much smaller semi-circle, which reflected higher conductivity and low charge transfer resistance on the electrode structure, respectively; this leads to a faster ion transfer, which boosts the capacitance [70]. To quantitatively evaluate all of these aspects in the impedance spectrum, the overall spectrum was fitted by an equivalent circuit (shown in the inset of Figure 9) [71], known as the modified Randles circuit, that reproduces the straight line in the low frequency by the incorporation of a Warburg component in the circuit, and the depressed semicircle by a constant phase element (CPE), while resistors R_1 and R_2 reproduce the bulk resistance (R_1) and the charge transfer resistance (R_2–R_1).

The low values for R1 (see inset of Figure 9) confirm that both experimental systems (before and after continuous use) preserve low bulk resistance with prevailing resistance attributed to the biochar, which is minimally affected by the poor cycling performance of the conducting polymers. A general variation in the charge transfer resistance (R2) is observed for both experimental systems after successive uses, while an overall decrease in CPE value is observed with a stronger reduction in the response of the PPy-based device due to the characteristic lower cyclability attributed to pseudocapacitance-based materials

4. Conclusions

In this work, sustainable biomass electrode materials were prepared and employed in supercapacitors. A biomass-modified electrode with PPy was fully evaluated in terms of physicochemical and electrochemical features. The physicochemical characterization revealed that the PPy modification affected biochar morphology, specific surface area, pore structure, and the insertion of surface functionalities on the biochar's surface. The PPy loading reduced the electrode's specific surface area from 1052 $m^2\ g^{-1}$ to 87 $m^2\ g^{-1}$. Pseudocapacitive behavior prevails, with an improvement of 34% for areal capacitance. The wood-based electrodes delivered high areal capacitances of 282 and 370 mF cm^{-2} at 5 mA cm^{-2}, for pure biochar and biochar doped with PPy, respectively. At the end of 1000 cycles, the biochar doped with PPy had slightly reduced capacitance retention (72%) compared to pure biochar (92%). The improvement in the energy density and the areal capacitance for devices modified with polypyrrole confirm the relevant contribution of the conducting polymer on the overall pseudocapacitance behavior of the resulting supercapacitor.

Author Contributions: Conceptualization, R.M.A.P.L., G.S.d.R. and H.P.d.O.; Methodology, R.M.A.P.L. and G.S.d.R.; Validation, H.P.d.O.; Formal analysis, R.M.A.P.L. and G.S.d.R.; Investigation, R.M.A.P.L. and G.S.d.R.; Data curation, H.P.d.O.; Writing—original draft, R.M.A.P.L. and G.S.d.R.; Writing—review & editing, E.C.L., U.L., G.L.D.; Funding acquisition, E.C.L., U.L., G.L.D.; All authors have read and agreed to the published version of the manuscript.

Funding: Dr. dos Reis thanks Bio4Energy—a Strategic Research Environment appointed by the Swedish government and the Swedish University of Agricultural Sciences (SLU), for the funding support. This research was also funded by CAPES, FACEPE, FAPESB, and CNPq.

Data Availability Statement: Data can be made available upon request.

Acknowledgments: SLU, Bio4energy, CAPES, FACEPE, FAPESB, and CNPq. All authors thank the editors and anonymous reviewers for their valuable work.

Conflicts of Interest: The authors declare no conflict of interest.

References

1. Nirmaladevi, S.; Boopathiraja, R.; Kandasamy, S.K.; Sathishkumar, S.; Parthibavarman, M. Wood based biochar supported MnO_2 nanorods for high energy asymmetric supercapacitor applications. *Surfaces Interfaces* **2021**, *27*, 101548. [CrossRef]
2. Li, Y.; Zhu, L.; Shi, J.; Dou, Y.; Li, S.; You, R.; Zhang, S.; Miao, X.; Shi, S.; Ji, H.; et al. Super-hydrophilic microporous biochar from biowaste for supercapacitor application. *Appl. Surf. Sci.* **2021**, *561*, 150076. [CrossRef]
3. Khedulkar, A.P.; Dang, V.D.; Pandit, B.; Bui, T.A.N.; Tran, H.L.; Doong, R.-A. Flower-like nickel hydroxide@tea leaf-derived biochar composite for high-performance supercapacitor application. *J. Colloid Interface Sci.* **2022**, *623*, 845–855. [CrossRef] [PubMed]
4. Zhang, L.; Jiang, J.; Holm, N.; Chen, F. Mini-chunk biochar supercapacitors. *J. Appl. Electrochem.* **2014**, *44*, 1145–1151. [CrossRef]
5. Adhamash, E.; Pathak, R.; Qiao, Q.; Zhou, Y.; McTaggart, R. Gamma-radiated biochar carbon for improved supercapacitor performance. *RSC Adv.* **2020**, *10*, 29910–29917. [CrossRef]
6. Husain, Z.; Raheman, A.S.; Ansari, K.B.; Pandit, A.B.; Khan, M.S.; Qyyum, M.A.; Lam, S.S. Nano-sized mesoporous biochar derived from biomass pyrolysis as electrochemical energy storage supercapacitor. *Mater. Sci. Energy Technol.* **2022**, *5*, 99–109. [CrossRef]
7. Gupta, R.K.; Dubey, M.; Kharel, P.; Gu, Z.; Fan, Q.H. Biochar activated by oxygen plasma for supercapacitors. *J. Power Sources* **2015**, *274*, 1300–1305. [CrossRef]
8. Thines, K.; Abdullah, E.; Mubarak, N.; Ruthiraan, M. In-situ polymerization of magnetic biochar—Polypyrrole composite: A novel application in supercapacitor. *Biomass Bioenergy* **2017**, *98*, 95–111. [CrossRef]
9. Jiang, J.; Zhang, L.; Wang, X.; Holm, N.; Rajagopalan, K.; Chen, F.; Ma, S. Highly ordered macroporous woody biochar with ultra-high carbon content as supercapacitor electrodes. *Electrochim. Acta* **2013**, *113*, 481–489. [CrossRef]
10. Oliveira, G.d.S.; Candido, I.C.M.; Lima, R.M.A.P.; de Oliveira, H.P. All-In-One Energy Harvesting/Storage Integrated Systems Based on Eggshell Membranes. *ACS Appl. Electron. Mater.* **2022**, *4*, 4708–4718. [CrossRef]
11. Wu, Z.; Li, L.; Yan, J.-M.; Zhang, X.-B. Materials Design and System Construction for Conventional and New-Concept Supercapacitors. *Adv. Sci.* **2017**, *4*, 1600382. [CrossRef] [PubMed]
12. Vatansever, D.; Haciismailoglu, M. Pencil graphite/polypyrrole supercapacitors: The structural and chemical changes of the electrodes after capacitive measurements. *Mater. Chem. Phys.* **2023**, *295*, 127073. [CrossRef]
13. Jiang, H.; Sun, T.; Li, C.; Ma, J. Hierarchical porous nanostructures assembled from ultrathin MnO_2 nanoflakes with enhanced supercapacitive performances. *J. Mater. Chem.* **2012**, *22*, 2751–2756. [CrossRef]
14. Ji, W.; Ji, J.; Cui, X.; Chen, J.; Liu, D.; Deng, H.; Fu, Q. Polypyrrole encapsulation on flower-like porous NiO for advanced high-performance supercapacitors. *Chem. Commun.* **2015**, *51*, 7669–7672. [CrossRef] [PubMed]
15. Liu, Y.; Peng, X. Recent advances of supercapacitors based on two-dimensional materials. *Appl. Mater. Today* **2017**, *8*, 104–115. [CrossRef]
16. Baboukani, A.R.; Khakpour, I.; Drozd, V.; Allagui, A.; Wang, C. Single-step exfoliation of black phosphorus and deposition of phosphorene *via* bipolar electrochemistry for capacitive energy storage application. *J. Mater. Chem. A* **2019**, *7*, 25548–25556. [CrossRef]
17. Orlando, J.D.; Lima, R.M.A.P.; Li, L.; Sydlik, S.A.; de Oliveira, H.P. Electrochemical Performance of N-Doped Carbon-Based Electrodes for Supercapacitors. *ACS Appl. Electron. Mater.* **2022**, *4*, 5040–5054. [CrossRef]
18. Jiang, Y.; Liu, Z.; Lv, Y.; Tang, A.; Dai, L.; Wang, L.; He, Z. Perovskite enables high performance vanadium redox flow battery. *Chem. Eng. J.* **2022**, *443*, 136341. [CrossRef]
19. Mao, C.; Chang, Y.; Zhao, X.; Dong, X.; Geng, Y.; Zhang, N.; Dai, L.; Wu, X.; Wang, L.; He, Z. Functional carbon materials for high-performance Zn metal anodes. *J. Energy Chem.* **2022**, *75*, 135–153. [CrossRef]
20. Dos Reis, G.S.; Larsson, S.H.; Mathieu, M.; Thyrel, M.; Pham, T.N. Application of design of experiments (DoE) for optimised production of micro- and mesoporous Norway spruce bark activated carbons. *Biomass Convers. Biorefinery* **2021**, *1*, 1–19. [CrossRef]
21. Saini, S.; Chand, P.; Joshi, A. Biomass derived carbon for supercapacitor applications: Review. *J. Energy Storage* **2021**, *39*, 102646. [CrossRef]
22. González-Hourcade, M.; dos Reis, G.S.; Grimm, A.; Dinh, V.M.; Lima, E.C.; Larsson, S.H.; Gentili, F.G. Microalgae biomass as a sustainable precursor to produce nitrogen-doped biochar for efficient removal of emerging pollutants from aqueous media. *J. Clean. Prod.* **2022**, *348*, 131280. [CrossRef]
23. dos Reis, G.S.; Guy, M.; Mathieu, M.; Jebrane, M.; Lima, E.C.; Thyrel, M.; Dotto, G.L.; Larsson, S.H. A comparative study of chemical treatment by MgCl2, ZnSO4, ZnCl2, and KOH on physicochemical properties and acetaminophen adsorption performance of biobased porous materials from tree bark residues. *Colloids Surfaces A Physicochem. Eng. Asp.* **2022**, *642*, 128626. [CrossRef]

24. Guy, M.; Mathieu, M.; Anastopoulos, I.P.; Martínez, M.G.; Rousseau, F.; Dotto, G.L.; de Oliveira, H.P.; Lima, E.C.; Thyrel, M.; Larsson, S.H.; et al. Process Parameters Optimization, Characterization, and Application of KOH-Activated Norway Spruce Bark Graphitic Biochars for Efficient Azo Dye Adsorption. *Molecules* **2022**, *27*, 456. [CrossRef] [PubMed]
25. Le, T.-H.; Kim, Y.; Yoon, H. Electrical and Electrochemical Properties of Conducting Polymers. *Polymers* **2017**, *9*, 150. [CrossRef] [PubMed]
26. Kim, S.; Jang, L.K.; Park, H.S.; Lee, J.Y. Electrochemical deposition of conductive and adhesive polypyrrole-dopamine films. *Sci. Rep.* **2016**, *6*, 30475. [CrossRef]
27. Cao, Y.; Qi, X.; Hu, K.; Wang, Y.; Gan, Z.; Li, Y.; Hu, G.; Peng, Z.; Du, K. Conductive Polymers Encapsulation To Enhance Electrochemical Performance of Ni-Rich Cathode Materials for Li-Ion Batteries. *ACS Appl. Mater. Interfaces* **2018**, *10*, 18270–18280. [CrossRef]
28. de Oliveira, H.P.; Sydlik, S.A.; Swager, T.M. Supercapacitors from Free-Standing Polypyrrole/Graphene Nanocomposites. *J. Phys. Chem. C* **2013**, *117*, 10270–10276. [CrossRef]
29. Alcaraz-Espinoza, J.J.; De Melo, C.P.; De Oliveira, H.P. Fabrication of Highly Flexible Hierarchical Polypyrrole/Carbon Nanotube on Eggshell Membranes for Supercapacitors. *ACS Omega* **2017**, *2*, 2866–2877. [CrossRef]
30. Candido, I.C.M.; Oliveira, G.d.S.; Viana, G.G.; da Silva, F.A.G.; da Costa, M.M.; de Oliveira, H.P. Wearable Triboelectric Nanogenerators Based on Chemical Modification of Conventional Textiles for Application in Electrically Driven Antibacterial Devices. *ACS Appl. Electron. Mater.* **2022**, *4*, 334–344. [CrossRef]
31. Barakzehi, M.; Montazer, M.; Sharif, F.; Norby, T.; Chatzitakis, A. A textile-based wearable supercapacitor using reduced graphene oxide/polypyrrole composite. *Electrochim. Acta* **2019**, *305*, 187–196. [CrossRef]
32. Soleimani, M.; Ghorbani, M.; Salahi, S. Antibacterial Activity of Polypyrrole-Chitosan Nanocomposite: Mechanism of Action. *Int. J. Nanosci. Nanotechnol.* **2016**, *12*, 191–197.
33. Gao, M.; Wang, W.-K.; Zheng, Y.-M.; Zhao, Q.-B.; Yu, H.-Q. Hierarchically porous biochar for supercapacitor and electrochemical H_2O_2 production. *Chem. Eng. J.* **2020**, *402*, 126171. [CrossRef]
34. Ma, Z.-W.; Liu, H.-Q.; Lü, Q.-F. Porous biochar derived from tea saponin for supercapacitor electrode: Effect of preparation technique. *J. Energy Storage* **2021**, *40*, 102773. [CrossRef]
35. da Silva, R.J.; Lima, R.M.A.P.; de Oliveira, M.C.A.; Alcaraz-Espinoza, J.J.; de Melo, C.P.; de Oliveira, H.P. Supercapacitors Based on (Carbon Nanostructure)/PEDOT/(Eggshell Membrane) Electrodes. *J. Electroanal. Chem.* **2020**, *856*, 113658. [CrossRef]
36. Lima, R.M.A.P.; Alcaraz-Espinoza, J.J.; da Silva, F.A.G.; de Oliveira, H.P. Multifunctional Wearable Electronic Textiles Using Cotton Fibers with Polypyrrole and Carbon Nanotubes. *ACS Appl. Mater. Interfaces* **2018**, *10*, 13783–13795. [CrossRef] [PubMed]
37. Alcaraz-Espinoza, J.J.; de Oliveira, H.P. Flexible Supercapacitors Based on a Ternary Composite of Polyaniline/Polypyrrole/Graphite on Gold Coated Sandpaper. *Electrochim. Acta* **2018**, *274*, 200–207. [CrossRef]
38. Lima, D.R.; Lima, E.C.; Thue, P.S.; Dias, S.L.; Machado, F.M.; Seliem, M.K.; Sher, F.; dos Reis, G.S.; Saeb, M.R.; Rinklebe, J. Comparison of acidic leaching using a conventional and ultrasound-assisted method for preparation of magnetic-activated biochar. *J. Environ. Chem. Eng.* **2021**, *9*, 105865. [CrossRef]
39. Lima, R.M.A.P.; dos Reis, G.S.; Thyrel, M.; Alcaraz-Espinoza, J.J.; Larsson, S.H.; de Oliveira, H.P. Facile Synthesis of Sustainable Biomass-Derived Porous Biochars as Promising Electrode Materials for High-Performance Supercapacitor Applications. *Nanomaterials* **2022**, *12*, 866. [CrossRef]
40. dos Reis, G.S.; Lima, R.M.A.P.; Larsson, S.H.; Subramaniyam, C.M.; Dinh, V.M.; Thyrel, M.; de Oliveira, H.P. Flexible supercapacitors of biomass-based activated carbon-polypyrrole on eggshell membranes. *J. Environ. Chem. Eng.* **2021**, *9*, 106155. [CrossRef]
41. Thommes, M.; Kaneko, K.; Neimark, A.V.; Olivier, J.P.; Rodriguez-Reinoso, F.; Rouquerol, J.; Sing, K.S.W. Physisorption of gases, with special reference to the evaluation of surface area and pore size distribution (IUPAC Technical Report). *Pure Appl. Chem.* **2015**, *87*, 1051–1069. [CrossRef]
42. dos Reis, G.S.; Bergna, D.; Tuomikoski, S.; Grimm, A.; Lima, E.C.; Thyrel, M.; Skoglund, N.; Lassi, U.; Larsson, S.H. Preparation and Characterization of Pulp and Paper Mill Sludge-Activated Biochars Using Alkaline Activation: A Box–Behnken Design Approach. *ACS Omega* **2022**, *7*, 32620–32630. [CrossRef] [PubMed]
43. Zhou, H.; Han, G.; Xiao, Y.; Chang, Y.; Zhai, H.-J. Facile preparation of polypyrrole/graphene oxide nanocomposites with large areal capacitance using electrochemical codeposition for supercapacitors. *J. Power Sources* **2014**, *263*, 259–267. [CrossRef]
44. Jyothibasu, J.P.; Chen, M.-Z.; Lee, R.-H. Polypyrrole/Carbon Nanotube Freestanding Electrode with Excellent Electrochemical Properties for High-Performance All-Solid-State Supercapacitors. *ACS Omega* **2020**, *5*, 6441–6451. [CrossRef] [PubMed]
45. Dubal, D.P.; Lee, S.H.; Kim, J.G.; Kim, W.B.; Lokhande, C.D. Porous polypyrrole clusters prepared by electropolymerization for a high performance supercapacitor. *J. Mater. Chem.* **2012**, *22*, 3044–3052. [CrossRef]
46. Huang, T.; Zheng, B.; Kou, L.; Gopalsamy, K.; Xu, Z.; Gao, C.; Meng, Y.; Wei, Z. Flexible high performance wet-spun graphene fiber supercapacitors. *RSC Adv.* **2013**, *3*, 23957–23962. [CrossRef]
47. Liu, Y.; Wang, N.; Yang, C.; Hu, W. Sol–gel synthesis of nanoporous $NiCo_2O_4$ thin films on ITO glass as high-performance supercapacitor electrodes. *Ceram. Int.* **2016**, *42*, 11411–11416. [CrossRef]
48. Zhang, H.; Wei, J.; Yan, Y.; Guo, Q.; Xie, L.; Yang, Z.; He, J.; Qi, W.; Cao, Z.; Zhao, X.; et al. Facile and Scalable Fabrication of MnO_2 Nanocrystallines and Enhanced Electrochemical Performance of MnO_2/MoS_2 Inner Heterojunction Structure for Supercapacitor Application. *J. Power Sources* **2020**, *450*, 227616. [CrossRef]

49. Zhang, J.; Wang, Y.; Wu, J.; Shu, X.; Yu, C.; Cui, J.; Qin, Y.; Zhang, Y.; Ajayan, P.M.; Wu, Y. Remarkable supercapacitive performance of TiO_2 nanotube arrays by introduction of oxygen vacancies. *Chem. Eng. J.* **2017**, *313*, 1071–1081. [CrossRef]
50. Prasad, K.; Reddy, G.R.; Rajesh, M.; Babu, P.R.; Shanmugam, G.; Sushma, N.J.; Reddy, M.S.P.; Raju, B.D.P.; Mallikarjuna, K. Electrochemical Performance of 2D-Hierarchical Sheet-Like $ZnCo_2O_4$ Microstructures for Supercapacitor Applications. *Crystals* **2020**, *10*, 566. [CrossRef]
51. Li, Q.; Cheng, H.; Wu, X.; Wang, C.-F.; Wu, G.; Chen, S. Enriched carbon dots/graphene microfibers towards high-performance micro-supercapacitors. *J. Mater. Chem. A* **2018**, *6*, 14112–14119. [CrossRef]
52. Chen, Q.; Meng, Y.; Hu, C.; Zhao, Y.; Shao, H.; Chen, N.; Qu, L. MnO_2-modified hierarchical graphene fiber electrochemical supercapacitor. *J. Power Sources* **2014**, *247*, 32–39. [CrossRef]
53. Zhang, M.; Wang, X.; Yang, T.; Zhang, P.; Wei, X.; Zhang, L.; Li, H. Polyaniline/graphene hybrid fibers as electrodes for flexible supercapacitors. *Synth. Met.* **2020**, *268*, 116484. [CrossRef]
54. Park, J.; An, G.-H. Interface-engineered electrode and electrolyte for the improved energy-storing performance and stable mechanical flexibility of fibrous supercapacitors. *Appl. Surf. Sci.* **2021**, *549*, 149326. [CrossRef]
55. Lal, M.S.; Ramaprabhu, S. High Areal Capacitance of Flexible Supercapacitors Fabricated with Carbon Cloth-Carbon Fiber-TiO_2 Electrodes and Different Hydrogel Polymer Electrolytes. *J. Electrochem. Soc.* **2022**, *169*, 20514. [CrossRef]
56. Lu, J.; Ran, H.; Li, J.; Wan, J.; Wang, C.; Ji, P.; Wang, X.; Liu, G.; Hu, C. A Fast Composite-Hydroxide-Mediated Approach for Synthesis of 2D-$LiCoO_2$ for High Performance Asymmetric Supercapacitor. *Electrochim. Acta* **2020**, *331*, 135426. [CrossRef]
57. Shi, J.; Jiang, B.; Li, C.; Liu, Z.; Yan, F.; Liu, X.; Li, H.; Yang, C.; Dong, D.; Hao, J. Study on capacitance properties of the sputtered carbon doped titanium nitride electrode material for supercapacitor. *Vacuum* **2022**, *198*, 110893. [CrossRef]
58. Mane, S.M.; Teli, A.M.; Yang, H.K.; Kwon, E.; Nimbalkar, N.A.; Patil, D.R.; Shin, J.C. Nanoneedles anchored ultrathin petals of CuCo layered double hydroxide with high areal capacitance and long cycle life for high-performance hybrid supercapacitors. *J. Energy Storage* **2023**, *62*, 106941. [CrossRef]
59. Rustamaji, H.; Prakoso, T.; Devianto, H.; Widiatmoko, P.; Kurnia, K.A. Facile synthesis of N, S-modified activated carbon from biomass residue for promising supercapacitor electrode applications. *Bioresour. Technol. Rep.* **2023**, *21*, 101301. [CrossRef]
60. Li, K.; Liu, X.; Chen, S.; Pan, W.; Zhang, J. A flexible solid-state supercapacitor based on graphene/polyaniline paper electrodes. *J. Energy Chem.* **2019**, *32*, 166–173. [CrossRef]
61. Chen, C.; Qin, H.; Cong, H.; Yu, S. A Highly Stretchable and Real-Time Healable Supercapacitor. *Adv. Mater.* **2019**, *31*, e1900573. [CrossRef] [PubMed]
62. Wang, W.; Yang, Y.; Chen, Z.; Deng, Z.; Fan, L.; Guo, W.; Xu, J.; Meng, Z. High-performance yarn supercapacitor based on directly twisted carbon nanotube@bacterial cellulose membrane. *Cellulose* **2020**, *27*, 7649–7661. [CrossRef]
63. Sim, H.J.; Choi, C.; Lee, D.Y.; Kim, H.; Yun, J.-H.; Kim, J.M.; Kang, T.M.; Ovalle, R.; Baughman, R.H.; Kee, C.W.; et al. Biomolecule based fiber supercapacitor for implantable device. *Nano Energy* **2018**, *47*, 385–392. [CrossRef]
64. Yang, Z.; Zhao, W.; Niu, Y.; Zhang, Y.; Wang, L.; Zhang, W.; Xiang, X.; Li, Q. Direct spinning of high-performance graphene fiber supercapacitor with a three-ply core-sheath structure. *Carbon* **2018**, *132*, 241–248. [CrossRef]
65. Zhang, W.; Guo, R.; Sun, J.; Dang, L.; Liu, Z.; Lei, Z.; Sun, Q. Textile carbon network with enhanced areal capacitance prepared by chemical activation of cotton cloth. *J. Colloid Interface Sci.* **2019**, *553*, 705–712. [CrossRef]
66. Qi, K.; Hou, R.; Zaman, S.; Qiu, Y.; Xia, B.Y.; Duan, H. Construction of Metal–Organic Framework/Conductive Polymer Hybrid for All-Solid-State Fabric Supercapacitor. *ACS Appl. Mater. Interfaces* **2018**, *10*, 18021–18028. [CrossRef]
67. Bhargava, P.; Liu, W.; Pope, M.; Tsui, T.; Yu, A. Substrate comparison for polypyrrole-graphene based high-performance flexible supercapacitors. *Electrochim. Acta* **2020**, *358*, 136846. [CrossRef]
68. Moreno Araújo Pinheiro Lima, R.; de Oliveira, H.P. Carbon Dots Reinforced Polypyrrole/ Graphene Nanoplatelets on Flexible Eggshell Membranes as Electrodes of All-Solid Flexible Supercapacitors. *J. Energy Storage* **2020**, *28*, 101284. [CrossRef]
69. Hryniewicz, B.M.; Lima, R.V.; Marchesi, L.F.; Vidotti, M. Impedimetric studies about the degradation of polypyrrole nanotubes during galvanostatic charge and discharge cycles. *J. Electroanal. Chem.* **2019**, *855*, 113636. [CrossRef]
70. Soram, B.S.; Dai, J.; Kshetri, T.; Kim, N.H.; Lee, J.H. Vertically grown and intertwined $Co(OH)_2$ nanosheet@Ni-mesh network for transparent flexible supercapacitor. *Chem. Eng. J.* **2020**, *391*, 123540. [CrossRef]
71. Baboukani, A.R.; Khakpour, I.; Adelowo, E.; Drozd, V.; Shang, W.; Wang, C. High-performance red phosphorus-sulfurized polyacrylonitrile composite by electrostatic spray deposition for lithium-ion batteries. *Electrochim. Acta* **2020**, *345*, 136227. [CrossRef]